Cold spraying and laser cladding as an alternative to electroplating processes

Jaroslaw Sienicki
R&D Projects Office, Polskie Zaklady Lotnicze Sp z oo, Mielec, Poland
Wojciech Zórawski
Department of Mechatronics and Mechanical Engineering, Politechnika Swietokrzyska, Kielce, Poland
Adam Dworak
Polskie Zaklady Lotnicze Sp z oo, Mielec, Poland
Piotr Koruba
Faculty of Mechanical Engineering, Politechnika Wrocławska, Wroclaw, Poland
Piotr Jurewicz
Politechnika Wrocławska, Wroclaw, Poland, and
Jacek Reiner
Department of Mechanical, Politechnika Wrocławska, Wroclaw, Poland

Abstract

Purpose – The purpose of this paper is to propose cold spraying and laser cladding processes as alternatives to cadmium and chromium electroplating, respectively. There are many substances or chemicals within the coating technology that can be identified as substances of very high concern because of their carcinogenic or mutagenic nature. Cadmium and chromium undoubtedly belong to these items and are the basic constituents of electrolytic coating processes. Finding an alternative and adapting to the existing restrictions of the usage of such hazardous products stands for many to be or not to be in the market.

Design/methodology/approach – The research work was focused on down selecting the appropriate materials, producing the coating samples, testing their properties and optimizing process parameters by statistical method. On the one hand, the high-pressure cold spray system and spraying of the titanium coating on the landing gear component, and on the other hand, the high-energy laser cladding facility and the wear resistant cobalt-based coating deposited onto the shock absorber piston. Substrates of these two applications were made of the same material, 4330 – high-strength low-carbon steel.

Findings – Meeting the requirements of Registration, Evaluation, Authorization and Restriction of Chemicals implies undertaking research and implementation work to identify alternative processes. The work provides the technical characteristics of new coatings justifying application readiness of the researched processes.

Originality/value – Taguchi's design of experiment method was combined with the measurements and analysis of specified coating properties for the optimization of the cold spray process parameters. There is also laser cladding process development presented as a fast rate technology generating coatings with the unique properties.

Keywords Laser cladding, Cold spray, Deposition

Paper type Research paper

1. Introduction

The environmental problems and health risks connected with the use of cadmium and chromium result in an intensified search for alternatives to provide acceptable functional coatings with properties, such as corrosion protection and wear resistance, at a competitive cost.

Unlike electrolytic hard chrome plating (EHC), for which the problem lies in the release of hexavalent chrome in the deposition process, the issue with cadmium is the metal itself rather than its deposition technique. Therefore, then, any process that releases cadmium becomes inherently hazardous, exposing personnel and environment to danger. Cadmium is therefore a much more dangerous and common problem even in comparison with EHC because the toxic material is carried with the plated part throughout its life (Legg, 2000). Anyway, in relation to the European REACh Regulation (Registration, Evaluation, Authorization and Restriction of Chemicals) on toxic substances, both materials cadmium and hexavalent

The current issue and full text archive of this journal is available on Emerald Insight at: **www.emeraldinsight.com/1748-8842.htm**

Aircraft Engineering and Aerospace Technology
91/2 (2019) 205–215
© Emerald Publishing Limited [ISSN 1748-8842]
[DOI 10.1108/AEAT-01-2018-0071]

Received 21 January 2018
Revised 30 April 2018
Accepted 1 June 2018

chromium should be eliminated from the general use, including industrial-aircraft branch of protective coatings on steel elements.

The purpose of the European Commission seems to be fully justified; however, it implies serious consequences for many manufacturers and downstream users. Gradual (every two years) listing of the substances of very high concern in the Annex XIV to the REACh Regulation will in the near future result in the ban on placing them on the market and using them without permission in a specific direction of application. Cadmium and hexavalent chrome undoubtedly belong to these substances and are unchangeably the basic constituents of electrolytic coating processes used in the aviation sector which is the most demanding in terms of safety and quality management. Therefore, finding a new and economical solution stands for many, as well as for PZL Mielec – the Polish aircraft manufacturer, to be or not to be in the European market (Krześlak *et al.*, 2016, p. 1,066).

The aims of the Amphora Project that has been launched by PZL Mielec together with Polish Academies, Kielce University of Technology and Wroclaw University of Science and Technology, are directed toward the development of a new generation of protective coatings complying with environmental standards and the REACh directive. Of course, there are a number of cadmium and chromium electroplating alternatives now available but which is the right one for a particular application depends on what the coating is used for and then what are the critical properties that the alternative must have (Nawrat *et al.*, 2009, p. 209; Fasuba *et al.*, 2013, p. 128). The research work focused on powder deposition technologies and coatings applied on high-strength low-carbon steel substrates – 4330. The main tasks were focusing on selection of the appropriate coating materials and optimization of the process parameters for both technologies while keeping adopted criteria and requirements of these top-layers. On the one hand, cold spray system with high-pressure of propeller gas (up to 50 bar) and with anti-corrosion titanium coatings applied on aircraft landing gear components; on the other hand, high-energy (up to 4 kW) laser cladding system used for deposition of wear resistant coating intended for shock absorber piston surface. Both demonstrators are presented in Figure 1 as a part of the main landing gear of M28-05 aircraft made by PZL Mielec.

2. Cold spray as an alternative to electroplating cadmium

Electroplating with sacrificial cadmium causes absorption of hydrogen into steel substrate during the process. It can lead to an accelerated damage of the coated structures under load because of hydrogen embrittlement. Baking such components for the time up to 24 h at 200°C eliminates hydrogen, but it must take extra time and costs. The same requirement is a characteristic for electrolytic chrome plating. Another solution often met in automotive and building industries where corrosion protection is typically provided by zinc coating (galvanizing) is also not a viable option. Here again, hydrogen can be absorbed, but this time when zinc coating corrodes in service. This process is termed as hydrogen re-embrittlement (Agüero *et al.*, 2012, p. 229; Sabelkin *et al.*, 2016, p. 158). Cold spraying seems to be the best candidate to eliminate such threats. It has been proved that the process is able to cover structural substrates with various materials with no detrimental fatigue effect. The cold sprayed coatings are supposed to have no phase changes, good adhesion, minimum porosity and deposition at a very high manufacturing rate. The main advantage of the process is the elimination of unfavorable influence of temperature on the particles of the coating material and substrate. The coating is built by grains of powder hitting on a substrate with supersonic velocity (500 ÷ 1,200 m/s). These grains undergo large deformation, which consequently causes close adhesion of the deformed particles to substrate and to each other. In theory, particles travel at a minimum required velocity called critical velocity, and upon impact, particles deform at very high strain rate. During deformation, thermal softening dominates over work hardening in the impact area. The material jet is produced, which removes oxides from the surface of the covered materials and metal-to-metal bonding is created (Klinkov *et al.*, 2005, p. 582). Extensive research shows that bonding is a result of adiabatic shear instability and mechanical interlocking (Grujicic *et al.*, 2004, pp. 681-688). The particle velocity is affected by numerous factors. These can be divided into two groups. One comprises the properties of the powder material, size of powder particles, their morphology and surface oxidation, properties of the substrate and particle temperature prior to the moment of impact onto the surface. The other group comprises the process parameters, i.e. gas type, gas temperature and pressure, nozzle geometry, standoff

Figure 1 M28-05 Aircraft and landing gear components – Amphora project demonstrators

distance, spray angle and gun travel speed. Many studies focus on the optimization of these parameters to obtain the best coating properties and high-deposition efficiency (Assadi *et al.*, 2011, p. 1,164).

Manufacturing of the Ti protective coating meeting the required properties is a major research challenge of this work. Demands for coating alternative to cadmium were determined as follows: thickness up to 500 μm, hardness above 50 HV, tightness, cracks resistance and no detrimental influence on the base material during load.

The cold spray process development follows the stages illustrated in Figure 2.

2.1 Cold spray methodology

The experimental coatings were produced from commercially pure (CP) non-spherical (irregular) titanium powders with particle size distribution between (+20 −63 μm). Layers were deposited using nitrogen gas onto Ni-Cr-Mo low-carbon alloy called high-strength steel 4330 (50 HRC; Rm = 1,600 MPa) with four coating layers. During the cold spraying process, the following equipment was used: Impact Innovations 5/8 cold spray system (power – 34 kW; process gases – N_2 and He; max. gas pressure – 50 bar; max. gas temperature – 800°C). The system was coupled with the robotized station of Fanuc M-20iA and the positioner, all presented in Figure 3. The silicon carbide (SiC) nozzle was being cooled down during the process by water-cooling circulation, the installation being integrated with the system.

The samples dimensions were of 400 × 30 × 6 mm. Two types of substrate surface preparation were performed prior to spraying. One of them was grit blasting with 30 grit of Al_2O_3 and the second type left the substrate in "as received" state. Particles microstructure, their morphology and prepared samples for spraying are presented in Figure 4.

All cold sprayed coatings were sectioned across the thickness and mounted in a mount epoxy, shown in Figure 5(a). The samples were then polished. No chemical etching was carried out, as it could cause surface roughness that would adversely

Figure 2 Stages of the technology readiness level (TRL) for titanium coating development

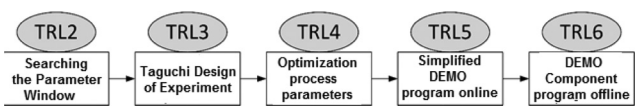

Figure 3 (a) Robot station for cold spray; and (b) process of the landing gear component

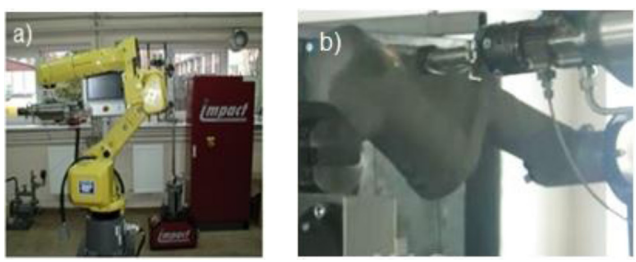

Figure 4 (a) Powder feedstock morphology; and (b) substrate samples

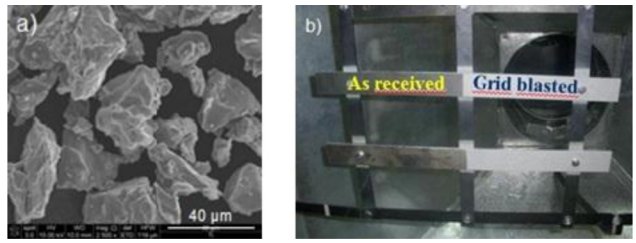

Figure 5 (a) Cross section mounted in a mount epoxy; and (b) porosity micrograph according to ASTM-E 2109

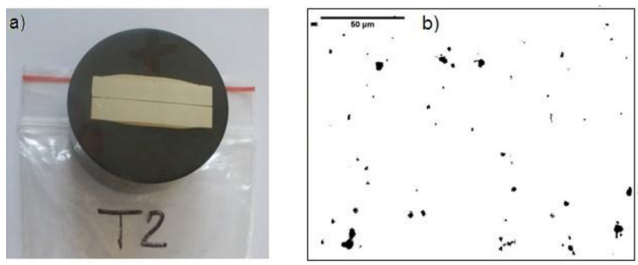

influence indentation and porosity measurements. Morphology of the powder feedstock, coatings microstructure and thickness and porosity were investigated on a cross section of coating–substrate system using scanning electron microscopy (SEM; Jeol JSM-7100 F; E-SEM FEI XL 30).

Coating porosity measurements, a total of 20 micrographs, were collected at 500× magnification, from which the average value was calculated according to ASTM-E 2109. Porosity was measured across the coating thickness 50 μm away from the interface and the surface top regions. The micrograph image can be seen in Figure 5(b).

Cold sprayed coatings demonstrate regions of high dislocation density and grain refinement and have varying amounts of defects such as porosity and particle boundaries (Ajaja *et al.*, 2011 p. 923).The extent of the defects and its character are not usually constant within a coating structure; therefore, the material is very challenging for hardness testing, and indentation size effect (ISE) must be taken into account during the measurements. Nanoindentaion tests were carried out using Nanovea system with a diamond Berkovitch tip (the Olivier and Pharr methodology). The survey of the hardness was performed with tree matrixes of 7 × 7 indents each with an indent spacing of 30 μm. The indentation map and the hardness distribution are presented in Figure 6. The load function had a 40 mN peak load and 100 mN/min loading and unloading rates. Decision of setting the load at such a high level was made basing on preliminary tests results (not reported here) where for varied loads the ISE, as a function of indentation load, was observed mostly at depths below 1 μm. At higher indentation depths, caused by higher loads, the ISE seemed to disappear and a nearly constant hardness was detected. Anyway, the true hardness or hardness at infinite indentation depth will always be lower than nanoindentaion measurements. The relationship between nanohardness and

Figure 6 (a) Nanohardness map; and (b) nanohardness histogram

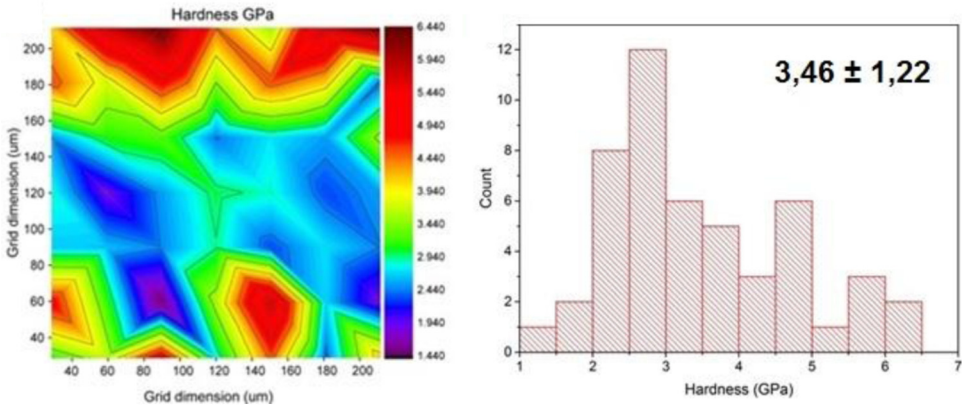

(a) (b)

indentation depth is well summarized by the theory of Nix and Gao (1998, p. 411).

Microindentation tests were conducted with a Vickers diamond indenter with the load of 0.3 N. Five indents, spaced at ten-indent spacing were performed at the same load. Diagonals were measured by optical means with magnification of 500×. At this scale, microscopic defects, mainly porosity and de-bonding between particles, could also affect indentation measurements. These defects increase indent size resulting in a decrease in microhardness. Microindentation hardness values in the study were measured in HV units and then were converted into the units of GPa. Because both indenters (Berkovich and Vickers) are self-similar with a nearly identical relationship between projected area and indentation, depth measurements made by both techniques are found to have good compatibility and their results comparison could take place.

2.2 Cold spray experimental procedure

Model spray analysis shows that output parameters (here coating properties) cannot be explicitly determined without input parameters because of the influence of occurring interfering factors; that is why, spraying is a stochastic process. Optimization therefore required application of a statistical method in the design of experiment (DoE) procedure. The aim of the DoE was to optimally use and control all the independent input parameters called control factors to determine the best settings for each of them, so that the required coatings properties could be achieved. Taguchi's multifactor experiment was used to achieve this goal. Taguchi suggested a specially designed method called the use of orthogonal array to study the selected parameter space with lesser number of experiments to be conducted. He recommends the use of the loss function to measure performance characteristics that are deviating from the desired target value. The value of this loss function is further transformed into signal-to-noise (S/N) ratio.

To identify the control factors and their levels, four cold spray process input parameters were selected, P = 4, and each varied at tree levels, as provided in Table I. The variables were as follows: process gas temperature (ranging from 700°C ÷ 800°C), process gas pressure (between 30 ÷ 42 bars), gun–substrate standoff distance (between 30 ÷ 50 mm) and finally the gun travel speed (varying within 300 ÷ 500 mm/s). The parameters' levels define the experimental region. Other input parameters that also influence largely are coating properties but, in this study, remained unchanged, and were taken as constants, e.g. the process gas type, qualities of substrate (hardness, thermal coefficient, surface preparation), powder feeding rate (speed disc) 2 rpm, nozzle orientation angle 90° and step distance 2 mm. All parameters were selected on the base of limitations of the equipment used.

The suitable orthogonal array L9 (34) and the corresponding matrix experiment generated nine deposition conditions to be carried out. The additional tenth process was also planned to be performed as a result of optimization.

The matrix experiment is presented in a cube form, shown in Figure 7, which clearly illustrates the experimental layout with the selected values of the factors, as well as determines the scope of the work.

Conducting the experiments allow to determine the influence of the selected input parameters (T– temperature; P – pressure; D – distance; and V – velocity) on specific coating properties such as thickness which corresponds deposition efficiency; porosity which reflects corrosion resistance; and nanohardness and microhardness that describes mechanical behavior. On the basis of Taguchi's criterion, all of the measured properties, except porosity, come under the category of being "the larger-the-better" type because both thickness and hardness in the study were desired to be as "large" as possible. Taguchi's signal to noise (S/N) ratio, also designated by η (Eta), takes both the average and variation into account. For this type of problem, there is equation (1):

$$\eta = -10 \quad \log_{10} \left(\frac{1}{n} \sum_{i=0}^{n} \frac{1}{y_i^2} \right) \tag{1}$$

where y_i is the quality characteristic that represents measurements of the analyzed properties, e.g. thickness or microhardness; and n is the number of measurements per experiment.

Whereas, in case of porosity, the situation is opposite; a protective coating should have as low microstructure porosity as possible to become fully functional. That kind of problem is

Table I Selected factors and their levels

Level	Temperature T (°C)	Pressure P (bar)	Standoff D (mm)	Traverse speed V (m/s)
1	T1	P1	30	300
2	T2	P2	40	400
3	T3	P3	50	500

Figure 7 Experiment cube with the processes' conditions at the vertices

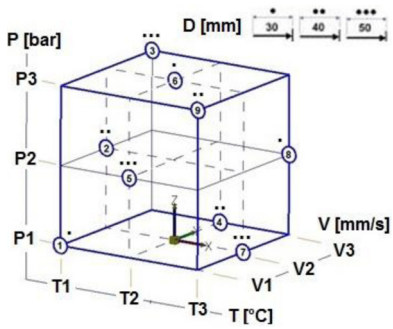

somewhat described by a different equation, equation (2) but with same representing symbols:

$$\eta = -10 \quad \log_{10} \left(\frac{1}{n} \sum_{i=0}^{n} y_i^2 \right) \tag{2}$$

The S/N ratio for each parameter level of each output property was estimated by averaging the S/N ratios obtained when the parameter was maintained at that level (Vijaya Babu *et al.*, 1996, p. 276).

Graphical representation of the S/N ratios obtained for different parameter levels are shown in Figure 8 for thickness and porosity and in Figure 9 for nanohardness and microhardness. In these figures, quantities of all measured coatings properties are also presented. η-graphs show the effects of changing the parameters from the lowest to the highest level (growing to the right). The greater the difference in the S/N ratio between the parameters' levels, the stronger the effect of parameter change on coating properties. The parameters levels at their maximum S/N ratios (circled on η-graphs) were considered as optimum for a particular coating property.

2.3 Cold spray results and discussion

Basically, it was easy and fast to obtain dense pure titanium coatings onto the 4330 substrate by spraying Ti powder within the selected window of process parameters. The coatings on substrates that had been grit blasted prior to deposition revealed significantly higher properties then coatings on "as received" substrates in every case. The layers of titanium formed a tight and homogeneous phase on the surface of all the samples. The strongest positive effect (i.e. the highest S/N ratio) on thickness had the gun travel speed set at the lowest rate.

The deposit thickness exceeded 600 μm for all coatings except for No 8. The highest speed rate in combination with the lowest standoff distance brought about decrease in deposition efficiency. The best efficiency was reported for samples No. 2 and No. 6 where the travel speed was 100 m/s higher in comparison to Nos 1, 5 and 9, but all of them had similar value level thicknesses. On coatings porosity and nanohardness, the most significant influence was exercised by gas temperature at the lowest level. It was a bit surprising. In general, higher gas temperature makes the particles velocity higher which consequently increases their plastic deformation on impact. It often positively influences porosity. For microhardness, the most important input parameter turned out to be the gas pressure. The highest values of microhardness were measured in coatings Nos 3, 6, 7 and 9. In these structures, the hardening process after particles deformation was the most intensive. The travel speed and the standoff distance could also play some role, but their significance was not so convincing because of that the respective max. S/N ratios were located within the error area on η-graphs – between dashed lines. While comparing the measurements of nanohardness (unaffected by porosity and particle boundaries) with microhardness (affected by micro-defects), there were distinct differences between their values. This is obvious that porosity and de-bonding of particles influence the mechanical properties. From that viewpoint, Sample no. 3 behaved the best. This is because of its high microhardness at the level of 203 HV (2.16 GPa) which corresponded with the lowest porosity value at 2.03 per cent and at same time with one of the highest values of nanohardness at 3.5 GPa. In fact, there was a smallest gap between microhardness and nanohardness which proved the lowest appearance of micro-defects inside Coating no. 3. The other coatings were much more affected by the defects, which could diminish their mechanical strength. What is particularly characteristic that the microhardness of the examined coatings increased with increasing of the gas pressure, whereas nanohardness decreased with increasing the gas temperature. The final step of the experiment was to conduct the last (tenth) deposition with the so-called "optimum averaged" of process parameters and to compare the obtained coating properties with the rest. The name "optimum averaged" comes from words synthesis. The predicted optimal levels of input parameters (max. S/N circled on η-graphs) of all tested properties were averaged or, better said, calculated as the weighted mean separately for gas temperatures, gas pressures, standoff distances and travel speeds. The overall formulas taken for the weight factor and for the "optimum averaged" were given, respectively, by equations (3) and (4):

$$w_i = \frac{|\eta_{max} - \eta_m|}{2 \times SE} \tag{3}$$

Figure 8 Experimental coatings results and η-graphs for thickness and porosity

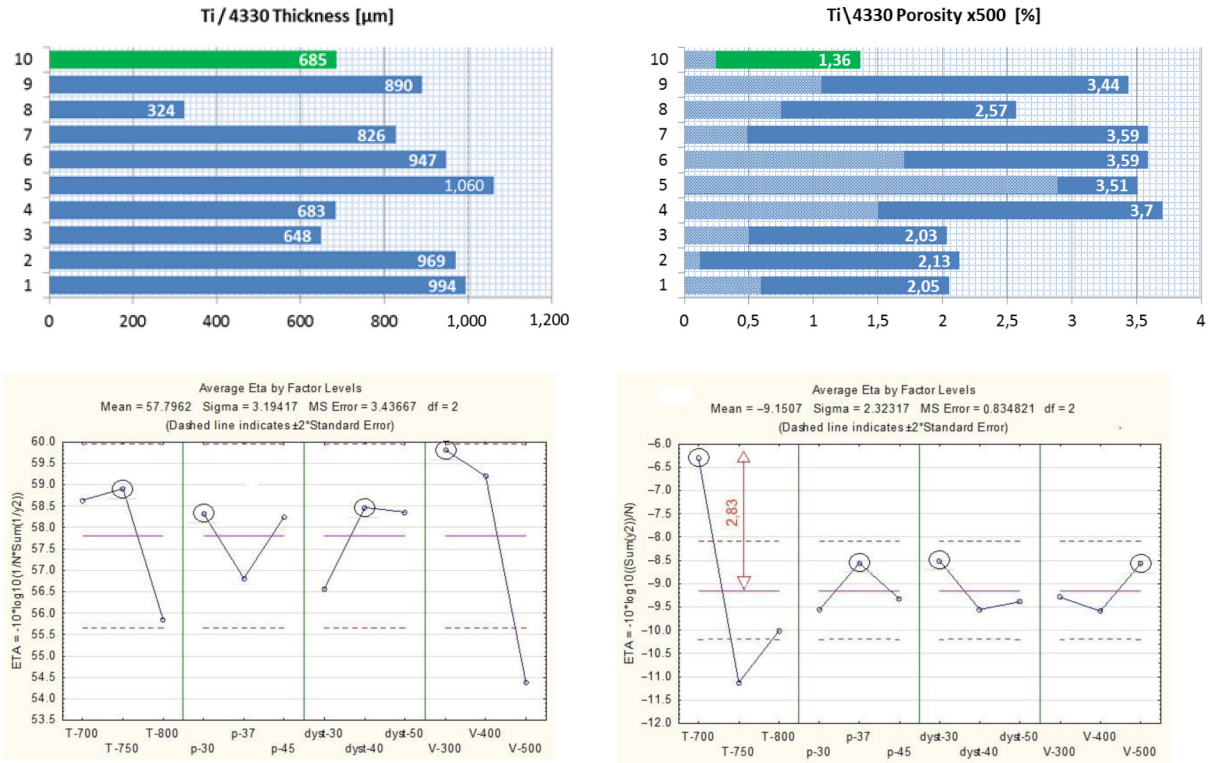

Figure 9 Experimental coatings results and η-graphs of nanohardness and microhardness

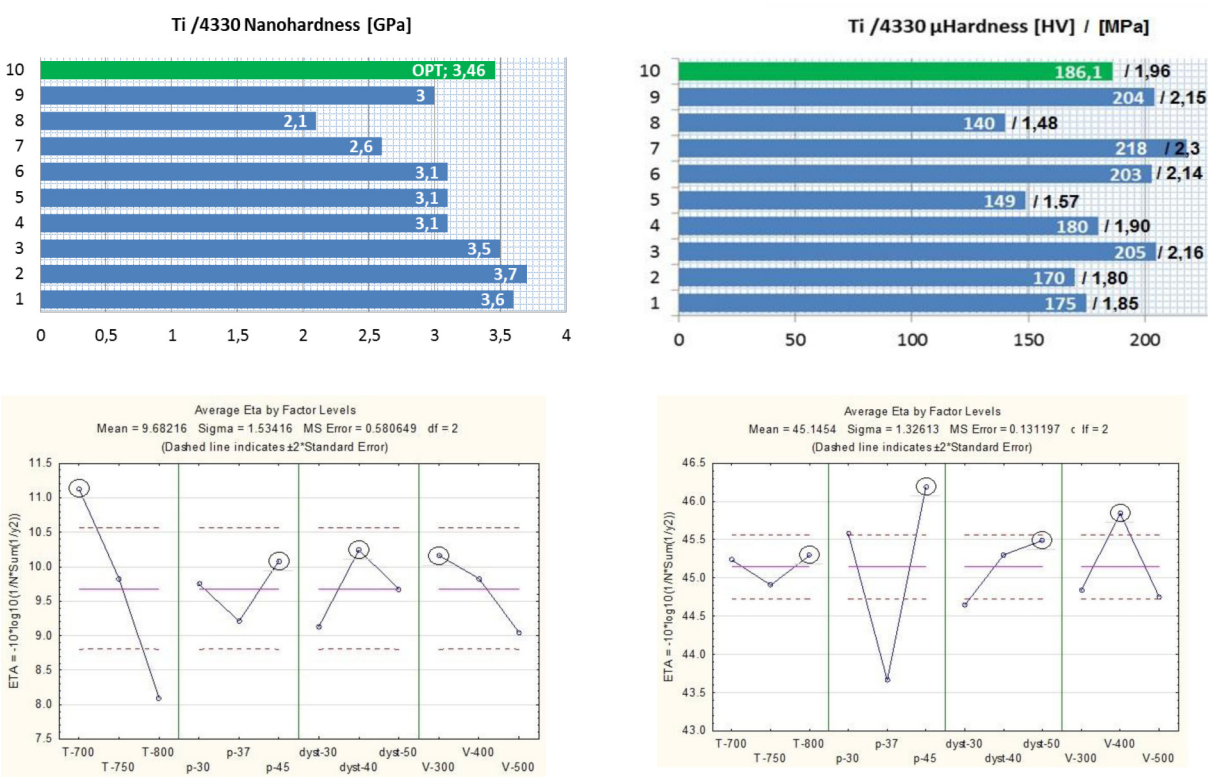

$$\overline{X}_{i(opt)} = \frac{\sum_{i=1}^{n} w_i \ X_i}{\sum_{i=1}^{n} w_i} \quad (4)$$

The factor (w_i) is the difference between the maximum S/N ratio (η_{max}) and the mean S/N ratio (η_m) – middle line on η-graphs which was determined in relation to standard error. The examples of calculations of gas temperature weight factor from the porosity η-graphs and the "optimum averaged" of the final gas temperature parameter were shown, respectively, by equations (5) and (6):

$$W_{T(por)} = \frac{|2.83 - 9.15|}{2 \times 0.52} = 2.68 \quad (5)$$

$$\overline{T}_{opt} = \frac{w_{T(por)} T_{(por)} + w_{T(th)} T_{(th)} + w_{T(nH)} T_{(nH)} + w_{T(\mu H)} T_{(\mu H)+}}{W_{T(por)} + W_{T(th)} + W_{T(nH)} + W_{T(HV)}} =$$

$$= \frac{2.68 \times 700 + 0.51 \times 750 + 1.63 \times 700 + 0 \times 800}{2.68 + 0.51 + 1.63 + 0}$$

$$= 705^{\circ}C \quad (6)$$

The "optimum averaged" of process parameters for conditions No. 10, shown in Figure 10, were placed into the cube nearby Coating no. 2. In comparison with this, the porosity of new coating decreased with an increased in the spraying distance and the gas pressure, respectively, by 10 mm and 6 bars.

This coating structure had small number of fine pores uniformly distributed over the entire thickness; it can be seen in Figures 5(b) and 11(a). Increased porosity was not observed in the outer layer of the coating. Similar changes occurring in cold sprayed coatings were reported by other researchers; the changes were because of the fact that the layers deposited last were not subjected to peening like the layers closer to the substrate which were deposited first. It can be assumed that the lower porosity of the outer layer of the coatings deposited at optimized parameters is attributable to very high velocity of particles, much higher than the critical value, which leads to a significant deformation of titanium particles also in the layer deposited last. Despite the high velocity of striking particles, the surfaces of all coating samples were very rough because of the use of powder with irregular particles; it can be seen in Figure 11(a).

Figure 10 Experimental cube with the "optimum averaged" of process parameters

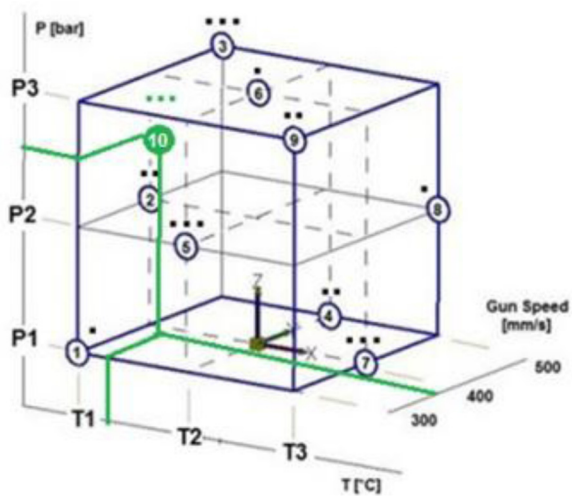

Axial fatigue strength according to ASTM E466 was carried out to determine if the Ti coating or coating application process modifies fatigue strength of substrate material.

A sinusoidal load of 20 Hz and load ratio R = −1 at room temperature (21°C) and 35 per cent humidity was applied. The fatigue experimental program shown in Table II was performed on round specimens of 10 mm diameter and 30-mm length of the gauge section presented in Figure 11(b) and (c).

There were two types of specimens examined; both were made of 4330 but coated separately by electrolytic plating and cold spraying with Cd and Ti, respectively. On reaching the predicted number of cycles, the test was stopped and specimens were taken out from the fatigue machine (computer-controlled servohydraulic axial machine) and subjected to nondestructive tests: one for top surface cracking appearance (examination of deposit structural integrity) and second for throughout porosity detection with ferroxine indicator {K3Fe(CN)6} according to AMS 2460. Both coatings passed the tests. There was no cracking or leakage detected in the coating structures which is noticeable, respectively, in Figure 12(a) and (b). Displayed specimens were examined after submitting to 100,000 fatigue cycles.

3. Laser cladding as alternative for electroplating hard chromium

Laser cladding process is commonly used to enhance surface properties such as hardness or wear resistance (pp. 592-599); and creep and corrosion resistance (Song *et al.*, 2018, pp. 357-369; Wang *et al.*, 2017, pp. 1116-1123) of many machine parts. During the process, laser serves as a heat source that melts the surface of the substrate creating a melt pool where, in case of cladding with powder, hit particles of additional material result in deposition of the clad. Using laser beam as a heat source allows obtaining fine microstructure, low dilution (high material purity) and a small heat affected zone (HAZ) in the deposit layer in comparison with other cladding technologies.

Before performing any experimental tests with laser cladding technology as the replacement of hard chromium plating, the specification of the desired coating properties had been determined. Electroplated chromium coatings are expected to have high corrosion resistance; high hardness and wear resistance; and tightness and low influence on base material. Demands for coating alternative to chromium were defined as follows: thickness 100-200 μm, hardness 550 ± 50 HV, minimal HAZ, operating temperature from −50°C up to +60° C and good corrosion resistance.

The laser cladding process development follows the stages illustrated in Figure 13.

3.1 Laser cladding methodology

In the described example, the substrate Ni-Cr-Mo low-alloy steel 4330 is regarded as easily weldable when the appropriate pre- and post-heat treatment was used.

During the laser cladding process, the following equipment, shown in Figure 14(a), were used: robot station RV60-40 with the external table RDK 05, laserline LDF 4000 laser unit,

Figure 11 (a) Cross section of the 10th; (b) Ti-coated fatigue test specimens; and (c) fatigue test

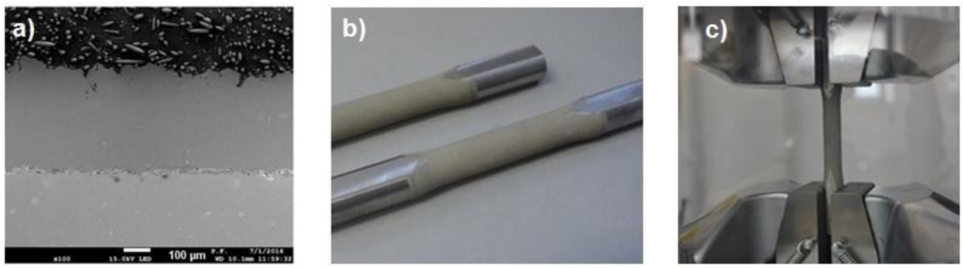

Table II Fatigue experimental program

Stress (MPa)	% σ_{us}	Predicted cycles	Cd/4330	Ti/4330
900	56	10,000	Passed no cracks/tight	Passed no cracks/tight
650	40	100,000		
550	34	500,000	-break at grip	-break at grip

Figure 12 (a) Top surface cracking appearance test; and (b) porosity test with ferroxine indicator

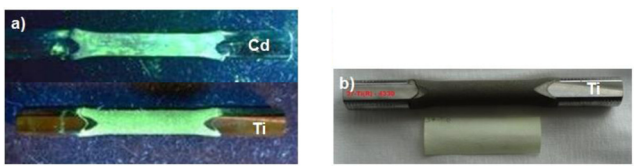

powder feeder GTV H-PF2/2 and COAXpowerline cladding nozzle. Moreover, a dedicated computer aided manufacturing software with workstation model was used for toolpath generation in manufacturing of samples and real-life component, seen in Figure 14(b).

To achieve properties of coating similar to hard chromium, a variety of additional materials can be used in laser cladding process. However, this number shrinks when weldability, price and compatibility with substrate are considered. These facts resulted in preparation of particular research plan for developing a new alternative coating with laser cladding technology. It is worth underlying that initial steps were used to select appropriate additional materials, whereas the later steps served as a verification of coating properties and its validation.

During the preliminary tests on single clads, the following materials were taken into account, wherein for each material the same set of process parameters was used:

- Tungsten carbides in co matrix (WOKA 3208);
- Laves phases in co matrix (Triballoy T-400, Triballoy T-800);
- Nickel-based self-fluxing NiCrBSi alloys (Metco 16C-NS, Metco 15F); and
- CoCr alloys with silicon and carbon (Stellite 1, Stellite 6).

On every single clad, visual and microhardness (HV 0.3) tests were conducted. Visual tests regarded the appearance of clad face (presence of welding imperfections) and clad cross-section (welding imperfections, layer height and penetration depth) shown in Figure 15(a) and (b). Microhardness was measured at three levels of the cross section and compared with the reference level of 550 HV. Each feature was rated from 1 to 5 points. The sum of rates allowed choosing three most promising materials for the next stage of development: Metco 16C-NS, Metco 15F and Stellite 6.

3.2 Laser cladding experimental procedure

For the initially chosen materials, the multi-clad layers were developed. A number of coatings with different process parameters were made for each material. Process parameters included variation of laser power, powder feed rate, travel speed

Figure 13 Stages of laser cladding coating development

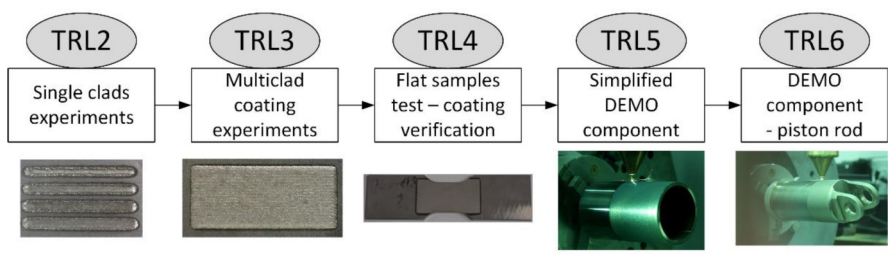

Figure 14 (a) Robot station for laser cladding; and (b) process of the real-life component

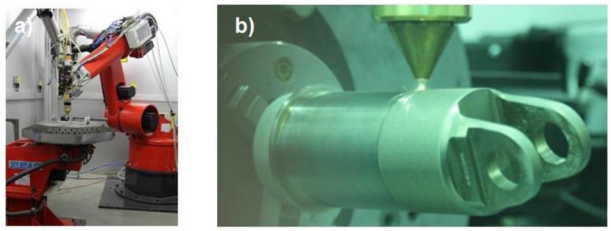

Figure 15 (a) Appearance of clad face – defects marked; and (b) cross section, hardness measurement points

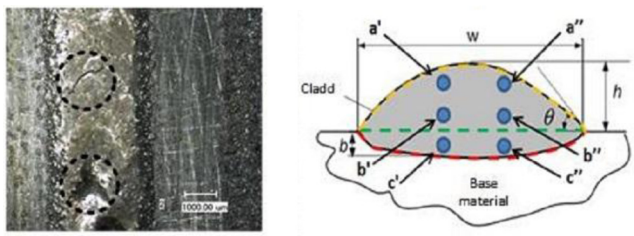

and overlap. Each coating face was further tested for presence of cracks, height, dilution and HAZ were measured in the cross section (perpendicular to cladding direction). The clad geometry parameters are noticeable in Figure 16.

In case of NiCrBSi alloy powder, the preheating of the substrate material was required to receive crack-free coatings. The preheating temperature for Metco 16C-NS was determined at 250°C, which is seen in Figure 17, in contrary to 350°C for Metco 15F, and therefore, the first alloy was chosen for further investigations. On the other hand, during laser cladding of Stellite 6, there was no point in preheating the substrate material, as no crack occurred.

The subsequent stage of alternative coating development consisted of preparations of two sets of flat samples for each additional material selected during experiments with multiclad coatings. A large variety of coating shapes on different substrate geometries, shown in Figure 18, was realized.

Table III shows groups of flat samples after the tests conducted with laser deposited coatings. It is worth mentioning that for every test the reference set of samples was prepared

Figure 16 Cross section of multiclad layer with measured geometrical properties

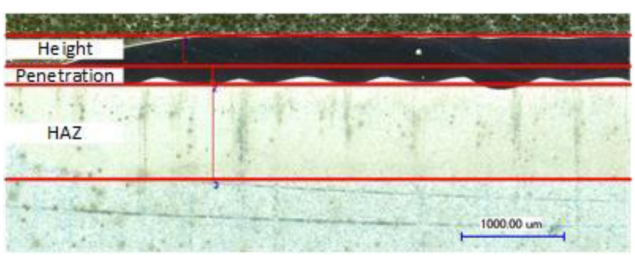

Figure 17 Crack detection by penetrant and influence of substrate preheating for Metco 16C powder

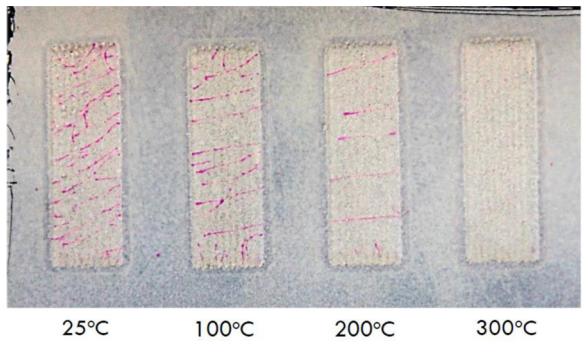

Figure 18 Variety of flat samples prepared for coatings verification

with hard chromium coating. In the case of mechanical properties, testing reference set of samples with no coatings at all were examined to define the influence of the coating deposition process on substrate material. For the purpose of this paper, only a few results shall be presented for an illustrative comparison of the coatings.

Research on the flat substrates showed that the travel speed was the most influential process parameter for improving coating hardness and HAZ depth reduction. The effort was made to achieve even higher velocities. However, it is more convenient to conduct such a process using cylindrical substrate and introduce it into rotational movement. Therefore, ultra-high speed laser cladding (UHSLC) technology may be regarded as development of conventional laser cladding, but in this case, cooling rates and coating properties are significantly higher (Schopphoven *et al.*, 2016). To perform UHSLC process, a particular workstation was developed consisting of small lathe coupled with the robot RV60-40 [5]. However, only the preliminary results of Stellite 6 coating deposition shall be presented further in case of more complex technological comparison.

3.3 Laser cladding results and discussion

Figure 19 shows the microstructure image of Stellite 6 coating (a) and Metco 16C (b) deposited on flat surfaces. In both cases, one can observe clear melting boundary between the cladding and the 4330 substrate. The microstructures of these clads consist of Cobalt (a) or Nickel (b) solid solution dendrites characterized by directional columnar growth. Inside the interdendritic spaces, a eutectic with separated carbides can be seen.

Table III Summary of tests performed on flat samples for coating verification

Geometric properties	Mechanical properties	Exploitative properties	Microstructure
Thickness before polishing	Tensile strength	Wear resistance (taber)	Cross-sections optical microscopy
Thickness after polishing	Fatigue	Loose abrasive wear test	Microhardness
Surface profile	Bending	Corrosion protection in salt fog	SEM microscopy
		Galvanic corrosion testing	Fractography
		Magnetic particle testing	

Figure 19 (a) Scanning electron microscopy images of the microstructure of Stellite 6; and (b) Metco 16C

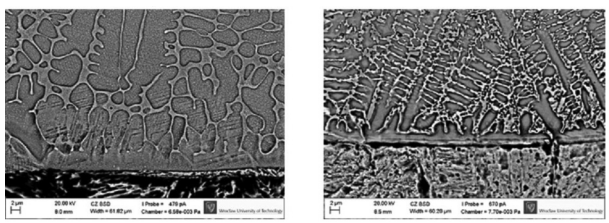

(a) (b)

In Table IV, the properties of electroplated hard chromium (EHC) and laser deposited coatings (LC – laser cladding) were gathered. From an operating point of view, it is necessary to compare wear and corrosion resistance of the deposited coatings. In case of wear resistance, a loose abrasive wear test was conducted according to GOST 23.208-79. The key parameter in this test is a relative abrasion index in comparison with a reference, which is the normalized C45 steel. A loose abrasive artificial corundum 90 (FEPA norm) was used. Second crucial test performed for cladded coatings was the potentiodynamic corrosion test according to ISO 17475. As a corrosive environment, a 3 per cent water solution of NaCl was chosen.

The results of the test indicated that because of additional preheating operation Metco 16C coatings were characterized by worse corrosion and wear resistance. Furthermore, in comparison with the Stellite 6, this coating had a tendency to crack even after many hours (cold cracking) and because of that the tightness of the coating was not ensured. As this feature is regarded as one of the most important, only Stellite 6 was used for further experiments on a cylindrical substrate. Moreover, Stellite 6 coating microhardness and wear resistance was regarded as sufficient, yet it still needs to be improved. On the other hand, it revealed much higher corrosion resistance than EHC coating. In the case of UHSLC technology, a multilayer coating was developed, which was characterized by lower dilution, lower HAZ depth and higher microhardness. Not only does the usage of UHSLC enhance the coating properties, but it also decreases processing time by about five times (Koruba *et al.*, 2017, pp. 15-19). However, UHSLC might be described as more sensitive to disturbances, and this is the reason for its further development.

4. Conclusions

The effects of gas temperature, gas pressure, standoff distance and gun travel speed on cold sprayed pure titanium coatings onto the 4330 landing gear material were investigated. All obtained coatings were characterized in terms of their thickness, porosity and hardness. The best set of input parameters were determined based on idea of "optimum averaged" which reflected the quantification of the parameters effect on the selected coatings properties.

Taguchi's method proved its efficiency and was found to be useful in obtaining the best parameters settings for cold spraying with reduced experimental efforts. After optimization, corresponding coating and cadmium reference were deposited separately on the 4330 specimens and characterized under fatigue load. Both coatings systems resisted the load and remained undamaged with tight and homogeneous structure. Ti coating was then successfully cold sprayed onto landing gear real-life component.

During experimental trials on a single clad, from the variety of materials, cobalt-based alloy Stellite 6 and NiCrBSi alloy Metco 16C were selected, but the latter needed substrate preheating operation to be performed (to 250°C) so as to prevent the coating from cracking. However, more complex testing involving corrosion and wear abrasion indicated that Metco 16C coating might be too susceptible for cracking even hours after the laser cladding process. On the other hand, Stellite 6 coating does not show any such tendency. In comparison with the EHC coating, it is characterized by about four times better corrosion resistance and acceptable wear

Table IV Comparison of coatings properties for EHC, LC and UHSLC processes

		Coating properties				
Process/material	Thickness (μm)	Penetration depth (μm)	HAZ depth (μm)	Microhardness (HV 0.3)	Relative abrasion index	Corrosion rate (μm/year)
EHC – reference	100 ÷ 200	–	–	600 ± 50	1.19	3.23
Stellite 6 – LC	187	51	582	571 ± 24	1.05	0.84
Stellite 6 – UHSLC	199 (3 layers)	15	288	793 ± 43	–	–
Metco 16C – LC	211	92	784	599 ± 41	1.03	32.90

resistance. The laser cladding with Stellite 6 of real-life component with dimensions of 300× Ø100 took 50 min. It is worth saying that by increasing cladding speed, a UHSLC technology was developed for Stellite 6 coating material. Applying UHSLC boosted the process time again and the coating properties and reduced the heat impact on the 4330 steel substrate.

In relation to cadmium and chromium plating, the methods of spraying and cladding seemed to be useful for components that are large and do not require a very smooth surface; however, grinding is allowed and possible. Deposition area is essentially unlimited, and the coating materials are processed at high rates. The coatings do not need additional processes like chromate conversion or dehydration. Surface preparation is also cost effective, for instance, there is no need for grinding the substrate prior to deposition, as it is required in chromium plating. The processes are suitable for landing gear components but should not be considered as a general Cd and EHC replacement because of main limitations such as rough top surface, line of sight method and relatively thick deposit.

References

Agüero, A., del Hoyo, J.C., García de Blas, J., García, M., Gutiérrez, M., Madueño, L. and Ulargui, S. (2012), "Aluminum slurry coatings to replace cadmium for aeronautic applications", *Surface & Coatings Technology*, Vol. 213, pp. 229-238.

Ajaja, J., Goldbaum, D. and Chromik, R. (2011), "Characterization of Ti cold spray coatings by indentation methods", *Acta Astronautica*, Vol. 69 Nos 11/12, pp. 923-928.

Assadi, H., Schmidt, T., Richter, H., Kliemann, J.O., Binder, K., Gärtner, F., Klassen, T. and Kreye, H. (2011), "On parameter selection in cold spraying", *Journal of Thermal Spray Technology*, Vol. 20 No. 6, pp. 1161-1176.

Fasuba, O.A., Yerokhin, A., Matthews, A. and Leyland, A. (2013), "Corrosion behaviour and galvanic coupling with steel of Al-based coating alternatives to electroplated cadmium", *Materials Chemistry and Physics*, Vol. 141 No. 1, pp. 128-137.

Grujicic, M., Zhao, C.L., DeRosset, W.S. and Helfritch, D. (2004), "Adiabatic shear instability based mechanism for particles/substrate bonding in the cold-gas dynamic-spray process", *Materials and Design*, Vol. 25 No. 8, pp. 681-688.

Klinkov, V.S., Fedorovich Kosarev, V. and Rein, M. (2005), "Cold spray deposition: significance of particle impact phenomena", *Aerospace Science and Technology*, Vol. 9 No. 7, pp. 582-591.

Koruba, P. Jurewicz, P. and Reiner, J. (2017), "Application of Ultra-High-Speed Laser Cladding (UHSLC) for functional coatings deposition in aviation industry", *Przegląd Spawalnictwa*, Vol. 89 No. 6, pp. 15-19.

Krześlak, A., Raga, K. and Sobkowiak, A. (2016), "Przemysł lotniczy w Polsce wobec wprowadzenia rozporządzenia REACH", *Przemysł Chemiczny*, Vol. 1 No. 6, pp. 1066-1071.

Legg, K. (2000), "Cadmium replacement alternatives for the joint strike fighter", Rowan Project #: 3105JSF3; Date: December 18, 2000.

Nawrat, G., Simka, W., Maciej, A., Nieużyła, Ł. and Orłowska, M. (2009), "Anticorrosive coatings alternate to cadmium coatings", *Ochrona Przed Korozją*, Vol. 2009 Nos 4/5, pp. 209-212.

Nix, W.D. and Gao, H. (1998), "Indentation size effects in crystalline materials: a law for strain gradient plasticity", *Journal of the Mechanics and Physics of Solids*, Vol. 46, pp. 411-425.

Sabelkin, V., Misak, H. and Mall, S. (2016), "Fatigue behavior of Zn–Ni and Cd coated AISI 4340 steel with scribed damage in saltwater environment", *International Journal of Fatigue*, Vol. 90, pp. 158-165.

Schopphoven, T., Geasser, A. and Wissenbach, K. (2016), "Investigations on ultra-high-speed laser material deposition as alternative for hard chrome plating and thermal spraying", *Journal of Laser Applications*, Vol. 28 No. 2.

Song, B., Voisey, K.T. and Hussain, T. (2018), "High temperature chlorine-induced corrosion of Ni50Cr coating: HVOLF, HVOGF, cold spray and laser cladding", *Surface & Coating Technology*, Vol. 337, pp. 357-369.

Vijaya Babu, M., Krishna Kumar, R., Prabhakar, O. and Gowri Shankar, N. (1996), "Optimization of flame spraying process parameters for high quality molybdenum coatings using Taguchi methods", *Surface and Coatings Technology*, Vol. 79 Nos 1/3, pp. 276-288.

Wang, S.L., Zhang, Z.Y., Gong, Y.B. and Nie, G.M. (2017), "Microstructures and corrosion resistance of Fe-based amorphous/nanocrystalline coating fabricated by laser cladding", *Journal of Alloys and Compounds*, Vol. 728, pp. 1116-1123.

Further reading

Assadi, H., Gartner, F., Stoltenhoff, T. and Kreye, H. (2003), "Bonding mechanism in cold gas spraying", *Acta Materialia*, Vol. 51 No. 15, pp. 4379-4394.

Sriramana, K.R., Brahimia, S., Szpunar, J.A., Osborne, J.H. and Yue, S. (2013), "Characterization of corrosion resistance of electrodeposited Zn–Ni, Zn and Cd coatings", *Electrochimica Acta*, Vol. 105, pp. 314-323.

Corresponding author

Jaroslaw Sienicki can be contacted at: jaroslaw.sienicki@lmco.com

For instructions on how to order reprints of this article, please visit our website:
www.emeraldgrouppublishing.com/licensing/reprints.htm
Or contact us for further details: **permissions@emeraldinsight.com**